



Planar optical waveguide for refractive index determining with high sensitivity and dual-band characteristic for Nano-sensor application

Fatemeh Tavakoli¹ · Sepideh Ebrahimi²

Received: 6 February 2019 / Accepted: 22 May 2019 / Published online: 25 May 2019
© Springer Science+Business Media, LLC, part of Springer Nature 2019

Abstract

In this paper, we develop an optical waveguide based on metal–insulator-metal as a refractive index sensor with dual-band feature and a high figure of merit (FOM) and sensitivity. In this model, we utilize a Z-shape slot based on two stubs model in both metal layers and this structure is placed over a dielectric layer of SiO₂ as a substrate for planar application in the optical systems. In addition, the parametric studies are used to clarifying the elements influence on controlling the transmission and working frequency to achieve a dual-band characteristic at 1550 and 3100 nm which is suitable for optical fiber application. In fact, the compound stubs technique is suggested to modify the resonances of the waveguide for dual-band attributes based on the transmission line model. We simulate this waveguide using the Finite Integrated Technique (FIT) method. It is supposed that the waveguide is filled by various materials with the different refractive indexes in the range of 1 to 1.5. We obtain the FOM for these materials while the Fano response provides high FOM about the 3800 RIU⁻¹ and the sensitivity is 1790 nm/RIU. Therefore, the compound stubs strategy help to improve the FOM factor in the optical waveguide.

Keywords Sensor · MIM · Optical waveguide · Fano · Figure of merit · Dual-band

1 Introduction

The Plasmonic behaviors have been considered for the optical and subwavelength devices such as Nano-antenna for improving the near field (Hosseinbeig et al. 2017; Zarrabi et al. 2016), Nano absorber for enhancing the electric field absorbing at solar cell (Nouri-Novin et al. 2019) or bio-sensor (Heydari et al. 2017) cloaking an object for invisibility (Nouri-Novin et al. 2018) and the optical waveguide as a sensor or optical filter (Ebrahimi et al. 2018). As a matter of fact, the optical waveguides have been developed in many formations and have been used as

✉ Sepideh Ebrahimi
sepideh.ebrahimi87@yahoo.com

¹ Department of Electrical Engineering, Science and Research Branch, Islamic Azad University, Tehran, Iran

² Department of Engineering, Islamic Azad University, Aligoudarz Branch, Aligoudarz, Iran

an optical transmission line based on nanoparticle arrays like a chain (Hadad and Steinberg 2010) or multi-layer structure with the graphene as a reconfigurable device (Zhou et al. 2014). Moreover, various structures with multilayer graphene have been considered as the refractive index as metasurface for making a tunable device (Xia et al. 2016, 2017, 2018).

However, today, the optical waveguides in the form of Metal-isolator-Metal (MIM) (Gao et al. 2016) have been noticed for the optical sensing (Zhan et al. 2016) such as detection of liquid material. The higher figure of merit (FOM) value is the main reason to use this kind of sensor (Zarrabi et al. 2018). For this goal, the structures with Fano response have been suggested based on a sharp variation of the transmittance for enhancing the FOM value (Paul and Ray 2017).

Various shapes of the slot have been developed to achieve the Fano shape for transmission (Zafar and Salim 2014) such as End-Coupled Cavities for multi Fano as an optical Nanosensor (Li et al. 2017), symmetry breaking (Chen and Yu 2014), comb line slot and rectangle cavity (Zhang et al. 2014), stub and groove resonator coupled as a refractive index sensor (Chen et al. 2015a), using a rectangular ring for higher sensitivity (Chen et al. 2015b), Slow-light-enhanced Plasmonic Mach-Zehnder interferometer sensors (Huang et al. 2016), multiple-ring shaped (Zeng et al. 2016), dual T-Shaped cavities side-coupled (Han et al. 2016) and circular cavity (Wang et al. 2016).

On the other hand, stub techniques have been recently considered for controlling the resonance of the optical waveguide based on matching technique (Pannipitiya et al. 2011a, b). Actually, we can control the impedance of a transmission line (TL) with stubs.

In this paper, we have presented a new symmetrical model of the optical waveguide with two branch line as a compound stub. The branch size is the best method to control the resonance frequencies and it provides dual-band characteristic for the prototyped sensor. This object is placed over the dielectric layer which is made it well-suited for fabrication. For calculating the figure of merit, we have assumed that the waveguide is filled with liquids. In brief, the prototype structure shows the dual-band characteristic with the high figure of merit value for materials in the range of 1 to 1.5.

2 Theory of design

In this proposed MIM waveguide based on surface Plasmon Polaritons (SPPs), the insulating layer of air with the refractive index of $n = 1$ and we have used the optical silver as the metal layer so that the effective dielectric constant is determined by the Drude model or we can use the practical Palik model in the CST microwave studio:

$$\epsilon_m(\omega) = \epsilon_\infty - \frac{\omega_p^2}{\omega(\omega + i\gamma)} \quad (1)$$

Here $\epsilon_\infty = 3.7$ is the dielectric constant at infinite frequency $\omega_p = 9.1$ eV is the bulk plasma frequency, ω is the angular frequency of incident light, and $\gamma = 0.018$ eV is the damping frequency (Farmani et al. 2018) which we can use for silver at the optical domain in the CST microwave studio. The propagation constant of SPPs is given by:

$$\beta_{spp} = n_{eff}k_0 = n_{eff} \frac{2\pi}{\lambda} \quad (2)$$

While the k_0 is the wave-number and $n_{\text{eff}} = \epsilon_m \epsilon_{\text{in}} / (\epsilon_m + \epsilon_{\text{in}})^2$ is the effective refractive index of the MIM waveguide.

Apparently, the slot and stubs features have been utilized to obtain the phase shift as given in Eq. 3, where the k_{spp} ($k_{\text{spp}}(\omega) = 2\pi n_{\text{eff}} / \lambda_0$) is the wavenumber of SPP waves and l_{eff} is for the effective length of the cavity.

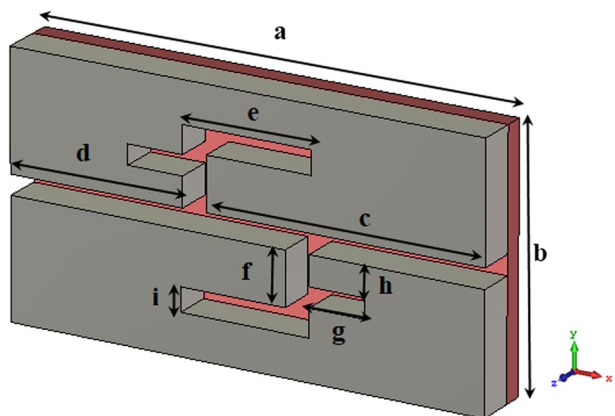
$$\Delta\varphi = k_{\text{spp}} \times l_{\text{eff}} = 2m\pi \quad (3)$$

Actually, we can model the plasmonic material based on Eq. 1 and we have used it for our simulation. Then the Eqs. 2 and 3 help us to define the slot for the prototyped MIM length.

3 Simulation design and modeling of the waveguide

Figure 1 shows the schematic structure of the proposed Plasmonic MIM waveguide structure, which contains two rectangular coupled sections. These metal layers make a waveguide and two Z-shaped (by compounding two stubs) slots with the double tooth-shaped cavity are implemented for controlling the resonances and designing an optical filter. In addition, the stub structure has been considered for developing the optical sensor (Pannipitiya et al. 2010). Moreover, this formation helps us to control the resonances with the dual-band in 1550 and 3100 nm. The two wave-ports are used for exciting the waveguide (designed sensor). The metal layers (Ag) are placed on the dielectric layer (SiO_2) as a substrate with a refractive index of 1.51. The waveguide is simulated by using CST microwave studio while the boundary condition is assumed to open and space with conventional PML and the mesh cells are assumed $N_x=101$ $N_y=44$ and $N_z=9$ while the simulation has been done by Time domain techniques. At least, all dimension of the prototyped waveguide are $a=1200$ nm, $b=650$ nm, $c=700$ nm, $d=440$ nm, $e=320$ nm, $f=135$ nm, $g=90$ nm, $h=75$ nm, $i=70$ nm.

Fig. 1 The geometry of the proposed MIM waveguide with the Z-shape slots for controlling of the resonances in 1550 and 3100 nm



4 Simulation results and discussions on parametric studies

The reflection and transmission of the proposed waveguide are presented in Fig. 2 for the suggested structure in the Fig. 1. As shown in Fig. 2, the transmission shows two resonances in 1550 and 3100 nm. So, it shows dual-band characteristic while the transmission at these wavelengths is around 0.001 for T0 which is important for the optical sensing. In addition, the transmission diagram shows the Fano shape can be supposed to improve the figure of merit of the prototype sensor. Moreover, the reflection value is increased up to 0.9.

As shown in Fig. 3a, we have checked the “e” (the length of the bigger stub) as the first parameter in the range of 225 to 265 nm with the step of 10 nm. As shown here, by increasing the “e” dimensions both resonances in 1550 and 3100 nm shift to a higher wavelength. At the first deep, the transmission value also reduced at 1600 nm when we have assumed the $e=265$ nm. However, it doesn’t have any effect on the second resonance transmission value. As a matter of fact, this parameter is the monumental factor for controlling the second resonance to obtain second harmonic attributes. So, this stub can utilize for modifying the first resonance and second resonance to modify the dual-band feature. Figure 3b shows the “g” (the length of the smaller stub) variations in the range of 60 to 140 nm with the step of 20 nm.

In here, also, by increasing the length of “g”, both resonances in 1550 and 3100 nm shift to a higher wavelength but at the first resonance at 1150 nm and when $g=140$ nm, we can see the higher wavelength shift ratio. However, it doesn’t have any effect on the transmission value. So, this stub can consider for controlling the first resonance. The next parameter is the “i” that is checked in Fig. 3c with the step of 10 nm from 20 to 60 nm. As shown here, by reducing the “i” dimensions, the first resonances at 1550 nm in comparison with the second resonance at 3100 nm has shifted to a higher wavelength with the higher ratio. Also, when we have assumed the “ $i=60$ nm” the transmission value increased at 1600 nm, but it doesn’t have any effect on the second resonance transmission value. As the last parameter, the “d” was examined and shown in Fig. 3d. In here, what changes of the “d” dimensions the diagram get less wide at the second resonance as we can see the peek at 1800 nm covers the broader area over 0.7. In the other side, this means that as the dimensions become larger it approaches a structure with a

Fig. 2 The transmission and reflection of the prototype waveguide with two resonances at 1550 nm and 3100 nm

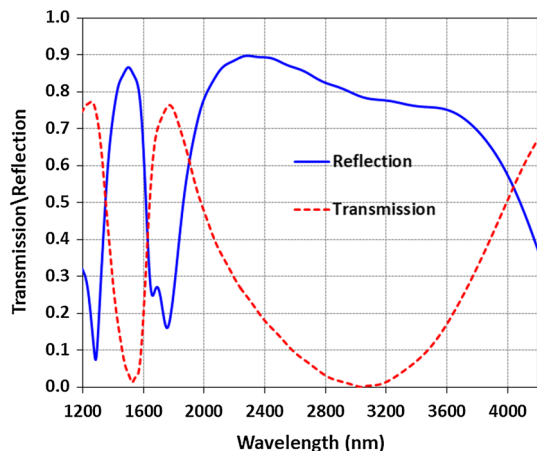
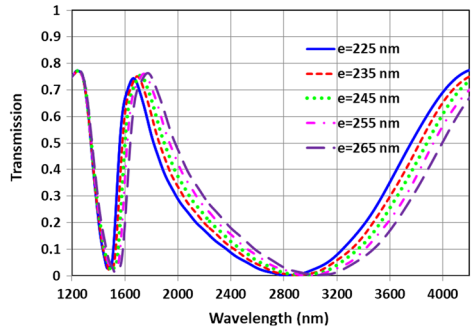
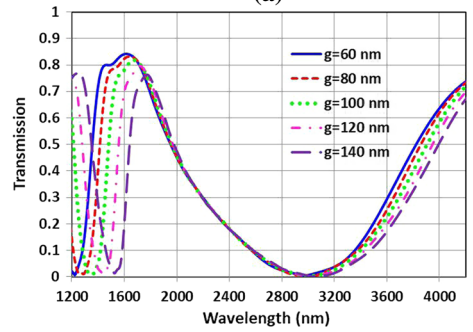


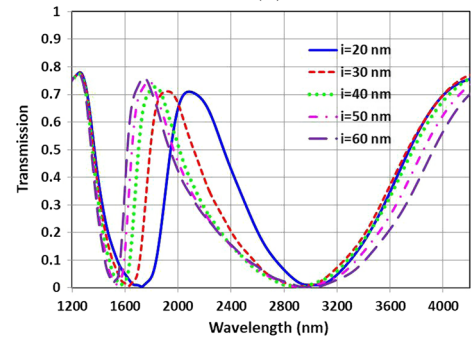
Fig. 3 The parametric studies of the prototyped waveguide for various elements of the structure **a** the effect of the bigger stub on transmission **b** the effect of the smaller stub on transmission **c** the width of the longer stub **d** the placement of the matching sections



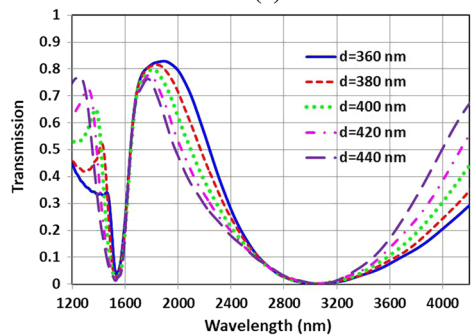
(a)



(b)



(c)



(d)

Fano response and given that we need to sharper changes to identify the material, the length of 440 nm is more attractive.

Various materials can be used as the substrate for making the practical model of the sensor while we have checked the Si ($n=3.53$), Si_3N_4 ($n=1.97$), and SiO_2 ($n=1.51$) as the substrate. As shown here, for the higher refractive index we have a red-shift. Exactly, the Si layer makes more shifts in comparison with SiN. As shown in Fig. 4, the SiO_2 substrate is more well-suited for the sensor which we can modify the resonance at 1550 nm for the optical fiber implementation.

The transmission line principles have been used for designing the optical coupled waveguide as a MIM waveguide while the Z_{MIM} is the impedance of the simple line which we can obtain by dividing the electrical with the magnetic field. Therefore, we can model the waveguide with a transmission line and its impedance can be obtained by Eq. 4. Where the β (h) is the SPP propagation constant, the η is the wave impedance in a vacuum, ϵ_1 is the relative permittivity of the dielectric which it is usually assumed 1 for the air, and $k=2\pi/\lambda$ (Pannipitiya et al. 2010) and the h is the height of the waveguide.

$$Z_{MIM}(h) = \frac{E_y}{H_z} = \frac{\beta(h)h\eta}{k\epsilon_1} \tag{4}$$

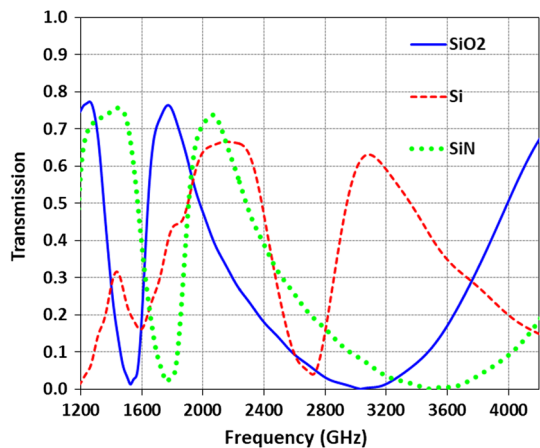
On the other hand, we can assume the $Z_{MIM}(w)$ for the stub line and it can be calculated by Eq. 5.

$$Z_S(w) = \frac{\beta(w)w}{\omega\epsilon_0\epsilon_1} \tag{5}$$

Obviously, the MIM waveguide looks like a transmission line with a certain impedance and length. For the matching circuit, the stub techniques have been suggested and Γ_{in} can obtain by Eq. 6 while the Z_L is the required impedance.

$$\Gamma = \frac{Z_L - Z_S}{Z_L + Z_S} \tag{6}$$

Fig. 4 Various material implementation as the substrate of the sensor with different refractive indexes



Therefore we can replace the stub line with Z_{stub} and we can obtain it by Eq. 7 while the Z_S and Z_L are achieved from Eqs. 5 and 6. Finally, based on the transfer matrix (Pannipitiya et al. 2011a), it is possible to define the equivalent circuit.

$$Z_{\text{stub}} = Z_S \frac{Z_L - iZ_S \tan(\beta l)}{Z_S - iZ_L \tan(\beta l)} \quad (7)$$

In addition, in our suggested model, we have used two stubs, so it is possible to obtain each line's impedance. Then, we can combine them as a single transmission line and we can use it for improving the matching of the conventional stub models which have been designed by Pannipitiya et al. (2010).

However, we should model the branches with transformers which can make the total Z_L by using Z_{L1} and Z_{L2} that are converted by the Eq. 7 and gathered.

Figure 5a and b shows the electric field distribution for two resonances at 1550 and 3100 nm, respectively and we have presented the basic model of the compound stub in Fig. 5c. As shown here, the smaller stub active at the lower wavelength at 1550 nm (198 THz) as shown in Fig. 5a. Where the bigger stub is useful for matching at a higher wavelength at 3100 nm (100 THz) as shown in Fig. 5b. Therefore, we can control the current distribution and effective length of the waveguide for modifying the frequency or wavelength. Here, the Eqs. 4 to 7 can be considered for modelling the prototype waveguide and also we can modify the final design by considering them.

5 Refractive index sensor application

There are important criterions for sensor designing, which are evaluated based on certain variables such as sensitivity, linearity, resolution, and hysteresis, dynamic range and figure of merit (FOM) (Rakhshani and Mansouri-Birjandi 2017; Zarrabi et al. 2018). When the biological material covers a structure, the reflection value, frequency shift and bandwidth will change. We can obtain the figure of merit (FOM) based on these variations, which is one of the main factors in Nano-sensor. Here, the FOM is defined by $\Delta T / (T \Delta n)$, while the “ T ” is the transmittance, “ ΔT ” is the transmittance variation induced by the refractive index change or “ Δn ” (Chen and Yu 2014). However, in some structures such as absorbers and Nano-antennas, the reflections have been considered for obtaining the FOM of the sensor (Zheng et al. 2017; Zarrabi et al. 2017). It should be noted that there is another method for calculating FOM as $\text{FOM} = \text{sensitivity (nm/RIU)}/\text{FWHM}$, which FWHM is full-width half-Maximum, but in MIM structures, the first method is often used because we can get more resolution.

We have checked the effect of various materials such as the liquids which are filled the inside of the waveguide. We have selected material with the refractive indexes in the range of $n=1$ to $n=1.5$. The transmission is checked for these materials and resented in Fig. 6. As shown in Fig. 6, we have a red-shift by increasing the refractive index of the material under test. We can achieve the maximum value of the FOM for $n=1.2$ and therefore, $\Delta n=0.2$, while the $\Delta T=0.75$ and $T=0.001$. So, we can obtain the $\text{FOM}=3800 \text{ RIU}^{-1}$ and the maximum sensitivity is 1791 nm/RIU for $\Delta n=0.1$ and the result for various refractive indexes are presented in Table 1.

We have compared this proposed MIM waveguide with some other previous models in Table 2 based on sensitivity and FOM factors. The results show that our structure has more FOM than some structures (Gao et al. 2016), while other structures

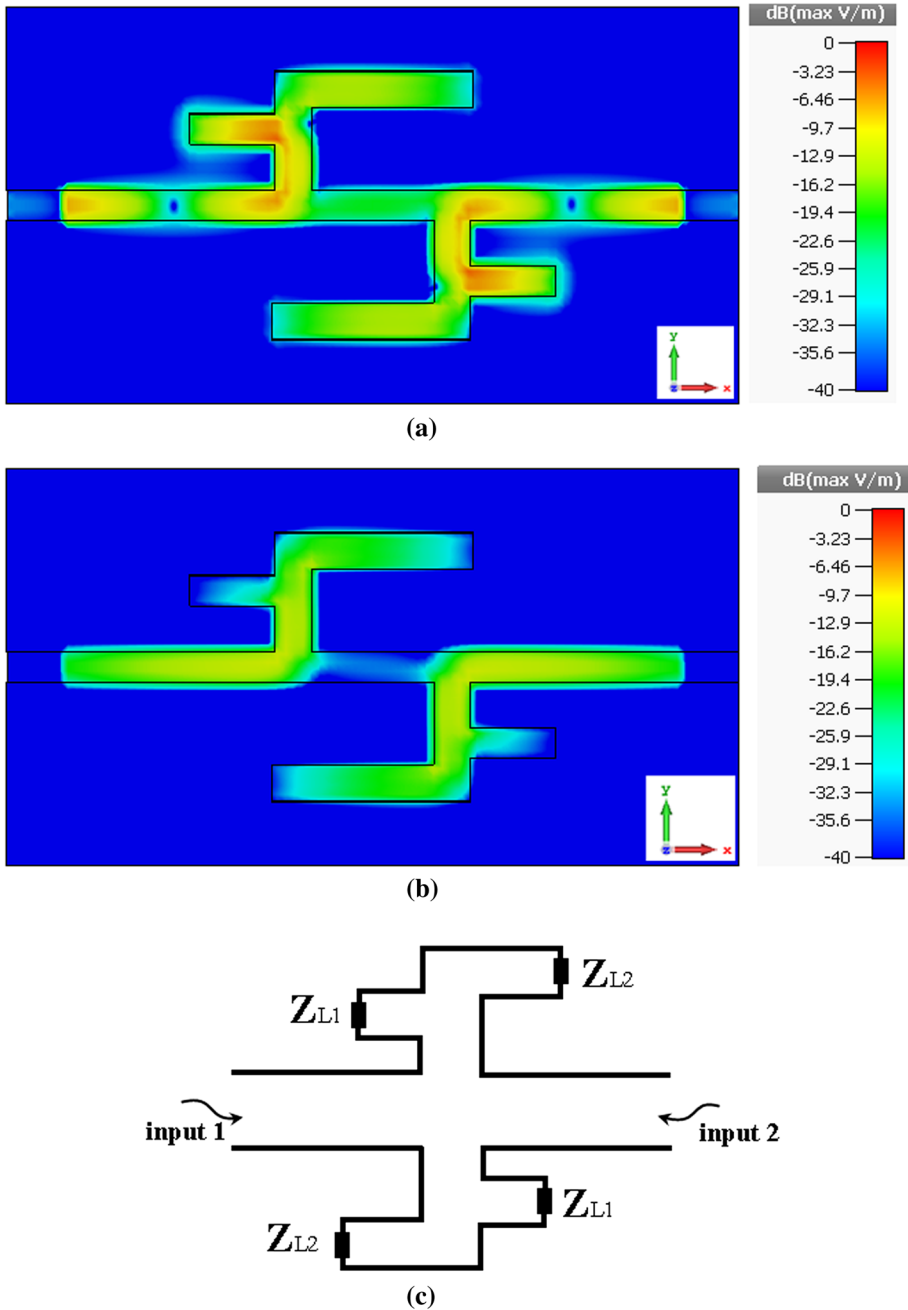
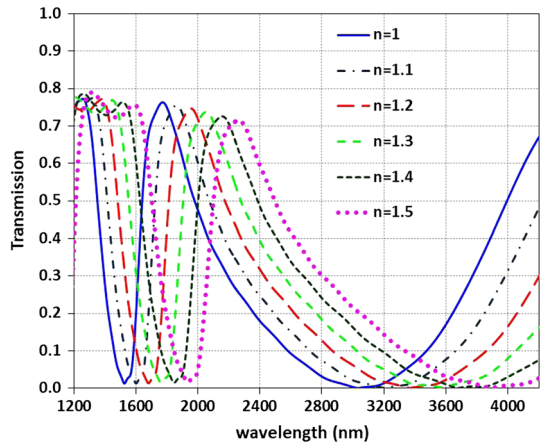


Fig. 5 **a** The current distribution of the suggested sensor at 1550 nm **b** the current distribution of the suggested sensor at 3100 nm **c** the equivalent circuit of the structure with dual stubs

Table 1 The sensitivity and FOM of the proposed MIM waveguide for $n=1$ to 1.5

	$n=1.1$	$n=1.2$	$n=1.3$	$n=1.4$	$n=1.5$
$\Delta\lambda_1$	66.4	145.75	288.35	305.6	424
S_1	663.9	728.8	761.2	763.9	848
FOM_1	1213.3	3804.95	2604.4	1927.9	1582.9
$\Delta\lambda_2$	179.2	323.4	470.8	677.2	833
S_2	1791.8	1616.85	1569.3	1693	1666
FOM_2	230.6	365	454.3	527.9	585.6

Fig. 6 the transmission of the waveguide with various materials for calculating the FOM**Table 2** comparing the proposed MIM waveguide with other models based on FOM, sensitivity and structure form

	FOM (RIU ⁻¹)	Sensitivity (nm/RIU)
This work	3804.95	1791.8
Zhan et al. (2016)	4800	–
Paul and Ray (2017)	277	–
Li et al. (2017)	2.73×10^4	1100
Chen and Yu (2014)	3.2×10^5	820
Chen et al. (2015a)	2.3×10^4	1260
Chen et al. (2015b)	6838	1300
Wang et al. (2016)	3.51×10^4	1450

have higher FOM with a maximum amount of 3.2×10^5 RIU⁻¹ (Paul and Ray 2017) than our structure. In addition, as we can see, our structure has a higher sensitivity of 1791.8 nm/RIU than other structures, so that for other structures, the maximum amount is 1450 nm/RIU (Huang et al. 2016).

6 Conclusion

In the current work, we have modeled a dual-band waveguide as a sensor with high FOM. We have obtained the maximum FOM value of 3800 RIU^{-1} at first resonances. The structure has two resonances at 1550 and 3100 nm. Actually, we have suggested novel form of slot for achieving the Fano resonance. This slot is based on compounding two stubs for matching the resonances as the parametric studies reveals that. The transmission line theory can be investigated by the electric field distribution inside of the MIM. In fact, in this proposed MIM waveguide, with the structure with dual stubs, as shown the parametric simulation results, we can improve resonances and transmission, which helps us to improve the FOM.

References

- Chen, Z., Yu, L.: Multiple Fano resonances based on different waveguide modes in a symmetry breaking plasmonic system. *IEEE Photonics J.* **6**(6), 1–8 (2014)
- Chen, Z., Li, Y., Wang, L., Duan, G., Zhao, Y., Xiao, J.: A refractive index nanosensor based on Fano resonance in the plasmonic waveguide system. *IEEE Photonics Technol. Lett.* **27**(16), 1695–1698 (2015a)
- Chen, Z., Cui, L., Song, X., Yu, L., Xiao, J.: High sensitivity plasmonic sensing based on Fano interference in a rectangular ring waveguide. *Opt. Commun.* **340**, 1–4 (2015b)
- Ebrahimi, S., Sabbaghi-Nadooshan, R., Tavakoli, M.B.: DNA implementation for optical waveguide as a switchable transmission line and memristor. *Opt. Quantum Electron.* **50**(4), 196 (2018)
- Farmani, A., Mir, A., Bazgir, M., Zarrabi, F.B.: Highly sensitive nano-scale plasmonic biosensor utilizing Fano resonance metasurface in THz range: numerical study. *Physica E Low Dimens Syst Nanostruct* **104**, 233–240 (2018)
- Gao, X., Ning, L., Liu, Z., Li, M., Ye, P., Chen, P., Li, M.: Optical filter effect of the metal–dielectric–metal waveguide with stub structure. *Optik Int. J. Light Electron Opt.* **127**(5), 2444–2447 (2016)
- Hadad, Y., Steinberg, B.Z.: Magnetized spiral chains of plasmonic ellipsoids for one-way optical waveguides. *Phys. Rev. Lett.* **105**(23), 233904 (2010)
- Han, X., Wang, T., Liu, B., He, Y., Zhu, Y.: Tunable triple plasmon-induced transparencies in dual T-shaped cavities side-coupled waveguide. *IEEE Photonics Technol. Lett.* **28**(3), 347–350 (2016)
- Heydari, S., Bazgir, M., Zarrabi, F.B., Gandji, N.P., Rastan, I.: Novel optical polarizer design based on metasurface nano aperture for biological sensing in mid-infrared regime. *Opt. Quantum Electron.* **49**(2), 83 (2017)
- Hosseinbeig, A., Pirooj, A., Zarrabi, F.B.: A reconfigurable subwavelength plasmonic fano nano-antenna based on split ring resonator. *J. Magn. Magn. Mater.* **423**, 203–207 (2017)
- Huang, Y., Min, C., Tao, S., Veronis, G.: Design of compact Mach–Zehnder interferometer-based slow-light-enhanced plasmonic waveguide sensors. *J. Lightwave Technol.* **34**(11), 2796–2803 (2016)
- Li, C., Li, S., Wang, Y., Jiao, R., Wang, L., Li, Y.: Multiple fano resonances based on plasmonic resonator system with end-coupled cavities for high-performance nanosensor. *IEEE Photonics J.* **9**(6), 1–9 (2017)
- Nouri-Novin, S., Zarrabi, F.B., Eskandari, A.-R., Naser-Moghadasi, M.: Design of a plasmonic absorber based on the nonlinear arrangement of nanodisk for surface cloak. *Opt. Commun.* **420**, 194–199 (2018)
- Nouri-Novin, S., Sadatgol, M., Zarrabi, F.B., Bazgir, Maryam: A hollow rectangular plasmonic absorber for nano biosensing applications. *Optik* **176**, 14–23 (2019)
- Pannipitiya, A., Rukhlenko, I.D., Premaratne, M., Hattori, H.T., Agrawal, G.P.: Improved transmission model for metal-dielectric-metal plasmonic waveguides with stub structure. *Opt. Exp.* **18**(6), 6191–6204 (2010)
- Pannipitiya, A., Rukhlenko, I.D., Premaratne, M.: Analytical modeling of resonant cavities for plasmonic-slot-waveguide junctions. *IEEE Photonics J.* **3**(2), 220–233 (2011a)
- Pannipitiya, A., Rukhlenko, I.D., Premaratne, M.: Analytical theory of optical bistability in plasmonic nanoresonators. *JOSA B* **28**(11), 2820–2826 (2011b)
- Paul, S., Ray, M.: Simultaneous switching at multiple wavelengths using plasmon induced transparency and fano resonance. *IEEE Photonics Technol. Lett.* **29**(9), 739–742 (2017)

- Rakhshani, M.R., Mansouri-Birjandi, M.A.: High sensitivity plasmonic refractive index sensing and its application for human blood group identification. *Sens. Actuators B Chem.* **249**, 168–176 (2017)
- Wang, Y., Li, S., Zhang, Y., Yu, L.: Ultrasharp Fano resonances based on the circular cavity optimized by a metallic nanodisk. *IEEE Photonics J.* **8**(6), 1–8 (2016)
- Xia, S.-X., Zhai, X., Wang, L.-L., Sun, B., Liu, J.-Q., Wen, S.-C.: Dynamically tunable plasmonically induced transparency in sinusoidally curved and planar graphene layers. *Opt. Exp.* **24**(16), 17886–17899 (2016)
- Xia, S.-X., Zhai, X., Huang, Y., Liu, J.-Q., Wang, L.-L., Wen, S.-C.: Graphene surface plasmons with dielectric metasurfaces. *J. Lightwave Technol.* **35**(20), 4553–4558 (2017)
- Xia, S.-X., Zhai, X., Wang, L.-L., Wen, S.-C.: Plasmonically induced transparency in double-layered graphene nanoribbons. *Photonics Res.* **6**(7), 692–702 (2018)
- Zafar, R., Salim, M.: Wideband slow light achievement in MIM plasmonic waveguide by controlling Fano resonance. *Infrared Phys. Technol.* **67**, 25–29 (2014)
- Zarrabi, F.B., Mohaghegh, M., Bazgir, M., Arezoomand, A.S.: Graphene–gold nano-ring antenna for dual-resonance optical application. *Opt. Mater.* **51**, 98–103 (2016)
- Zarrabi, F.B., Bazgir, M., Ebrahimi, S., Saeed Arezoomand, A.: Fano resonance for UI nano-array independent to the polarization providing bio-sensing applications. *J. Electromagn. Waves Appl.* **31**(14), 1444–1452 (2017)
- Zarrabi, F.B., Hekmati, R., Bazgir, M., Ebrahimi, S.: Nanoparticle using parallel split rings and implementation of chain for creating Fano resonance with polarization independence for energy harvesting in mid-infrared. *Opt. Quantum Electron.* **50**(12), 452 (2018)
- Zeng, Y.-P., Wang, L., Xia, X.-P., Wang, Z.-Y.: Research transmission characteristics of a plasmonic multiple-ring shaped metal-insulator-metal waveguide. *Optik Int. J. Light Electron Opt.* **127**(3), 1084–1086 (2016)
- Zhan, S., Peng, Y., He, Z., Li, B., Chen, Z., Hui, X., Li, H.: Tunable nanoplasmonic sensor based on the asymmetric degree of Fano resonance in MDM waveguide. *Sci. Rep.* **6**, 22428 (2016)
- Zhang, Z., Zhang, L., Li, H., Chen, H.: Plasmon induced transparency in a surface plasmon polariton waveguide with a comb line slot and rectangle cavity. *Appl. Phys. Lett.* **104**(23), 231114 (2014)
- Zheng, G., Zou, X., Chen, Y., Xu, L., Rao, W.: Fano resonance in graphene-MoS₂ heterostructure-based surface plasmon resonance biosensor and its potential applications. *Opt. Mater.* **66**, 171–178 (2017)
- Zhou, X., Zhang, T., Chen, L., Hong, W., Li, X.: A graphene-based hybrid plasmonic waveguide with ultra-deep subwavelength confinement. *J. Lightwave Technol.* **32**(21), 3597–3601 (2014)